

Article

# Observations of Atmospheric NO<sub>2</sub> Using a New Low-Cost MAX-DOAS System

Adrian Roșu<sup>1</sup>, Daniel-Eduard Constantin<sup>1,\*</sup> , Mirela Voiculescu<sup>1</sup> , Maxim Arseni<sup>1</sup>, Alexis Merlaud<sup>2</sup>, Michel Van Roozendael<sup>2</sup> and Puiu Lucian Georgescu<sup>1</sup>

<sup>1</sup> Faculty of Sciences and Environment, European Centre of Excellence for the Environment, “Dunarea de Jos” University of Galati, Domneasca Street, no. 111, 800201 Galati, Romania; Adrian.Rosu@ugal.ro (A.R.); mirela.voiculescu@ugal.ro (M.V.); Maxim.Arseni@ugal.ro (M.A.); georgescu.lucian@ugal.ro (P.L.G.)

<sup>2</sup> Royal Belgian Institute for Space Aeronomy (BIRA-IASB), Ringlaan-3-Avenue Circulaire, B-1180 Brussels, Belgium; alexis.merlaud@aeronomie.be (A.M.); michel.vanroozendael@aeronomie.be (M.V.R.)

\* Correspondence: daniel.constantin@ugal.ro

Received: 2 December 2019; Accepted: 21 January 2020; Published: 24 January 2020



**Abstract:** This article describes the prototype of a new MAX-DOAS (multi-axis differential optical absorption spectroscopy) system built at “Dunarea de Jos” University of Galati (UGAL), Romania, and the first results of its use to observe NO<sub>2</sub> content over Galati city (45.42° N, 28.04° E). The new equipment is a ground-based MAX-DOAS system capable of measuring the spatial distribution of DSCD (differential slant column densities) of several trace gases using horizontal and vertical observations. The new optic system, named UGAL-2-DOAS, is an in-house, low-cost, solution in comparison to the existing market of the MAX-DOAS systems. This paper describes the technical design and capabilities of the new MAX-DOAS instrument. The UGAL-2D-DOAS system was tested in April and June 2017 in Galati city. Measurements over three days were selected for the present manuscript. Full azimuthal (0–360°), local celestial meridian observations and other elevation angle sequence measurements (e.g., E–W) were performed. We found that the new MAX-DOAS system is able to detect diurnal variation and the local source emissions of NO<sub>2</sub> from the urban environment. Also, we present concomitant zenith-sky car-DOAS observations measurements around the location of the new MAX-DOAS instrument. Comparing the horizontal scanning sequence of the new developed instrument with the mobile DOAS observations, we found that both systems can indicate and detect the same NO<sub>2</sub> sources.

**Keywords:** UV–Vis spectroscopy; atmospheric remote sensing; nitrogen dioxide; MAX-DOAS; mobile DOAS

## 1. Introduction

The differential optical absorption spectroscopy (DOAS) technique is a remote-sensing detection method that uses scattered light to retrieve information about the abundance of several trace gases in the lower layers of the atmosphere. This measurement technique uses the transmitted ultraviolet–visible (UV–Vis) signal in active (artificial light source) and passive (natural sources e.g., Sun) applications. The first use of passive UV–Vis spectroscopy for measurements of atmospheric O<sub>3</sub> using a single spectral domain in zenith observations was performed by Dobson and Harrison in 1925 [1,2]. Early DOAS experiments used zenith-sky geometry for retrieving information about trace gases and aerosols in the troposphere and stratosphere [3]. Multiple axes were used initially in DOAS observations of tropospheric BrO and profiles of NO<sub>2</sub> [4,5]. The DOAS method enables the detection of trace-gases species like O<sub>3</sub>, NO<sub>2</sub>, SO<sub>2</sub>, HCHO, BrO, IO, OCIO and O<sub>4</sub> [4–10]. The combination between a large range of horizontal and vertical viewing directions led to a new DOAS technique, called MAX-DOAS (multi-axis differential optical absorption spectroscopy) [4,11].

The MAX-DOAS technique is an important remote-sensing measurement method which provides key information regarding vertical and horizontal distribution of atmospheric trace gases and aerosols [12]. The observations based on MAX-DOAS technique are spectra of the scattered sunlight recorded at different elevation angles or azimuthal directions, which can be used to calculate the abundance of atmospheric trace gases, based on the Beer–Lambert law [13–20]. Over the past two decades, the MAX-DOAS technique [9,11,13,15,16] has been used for atmospheric measurements as ground-based static or mobile observations. The MAX-DOAS observations can be performed using static or mobile observations from cars, unmanned aerial vehicles (UAV), ships, airplanes, etc. [21–24].

A mobile DOAS technique implemented as car-DOAS observations can be used for high-resolution horizontal observations of tropospheric NO<sub>2</sub> and other trace gases. Car-DOAS observations have been used for quantification of total emissions from urban or industrial emission sources [25,26], comparisons with satellite observations [27–29], validation of airborne DOAS measurements [30,31] and for comparisons with model simulations [29,32]. Also, car-DOAS measurements have recently been used for comparison with in situ measurements [33].

This paper describes a new MAX-DOAS instrument developed in-house at the “Dunarea de Jos” University of Galati (UGAL) and the first MAX-DOAS measurements of the NO<sub>2</sub> slant column over Galati city, Romania. The new instrument is considered a low-cost instrument due to the fact that the only expensive component of the system is the UV–Vis spectrometer. Also, a comparison between the observations of the new MAX-DOAS instrument and a zenith-sky car-DOAS system is presented. The work is organized as follows: data and methodology are described in Section 2, results and discussions are presented in Section 3, while Section 4 is dedicated to conclusions.

## 2. Methods and Data

### 2.1. Instrument Description

The new MAX-DOAS system, called UGAL-2D-DOAS, was developed in 2016–2017 at “Dunarea de Jos” University of Galati, Faculty of Science and Environment. Figure 1 shows the MAX-DOAS prototype mounted on a tripod, performing measurements at the experimental site (45.44° N, 28.05° E) on 11 April 2017.

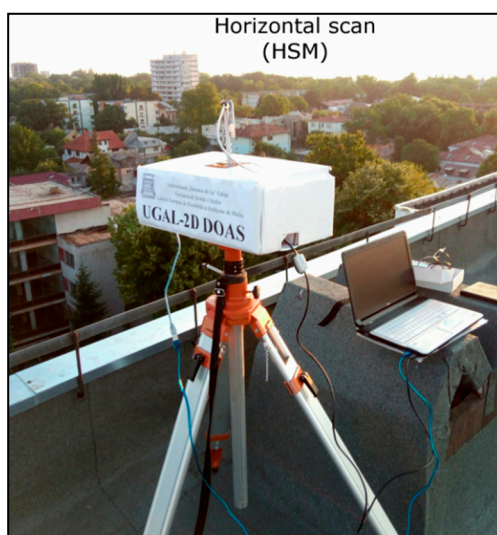


**Figure 1.** Image of the new University of Galati differential optical absorption spectroscopy (UGAL-2D-DOAS) system performing observations.

The measurement principle, which is similar to other MAX-DOAS instruments [34], is outlined in Figure 2a,b. The system can be used in two scanning modes: horizontal scanning mode (HSM), and vertical scanning mode (VSM). The horizontal scanning mode is capable to perform full azimuthal

(0–360°) observations, while the vertical scanning is able to perform local celestial meridian observations and other elevation angle sequence observations.

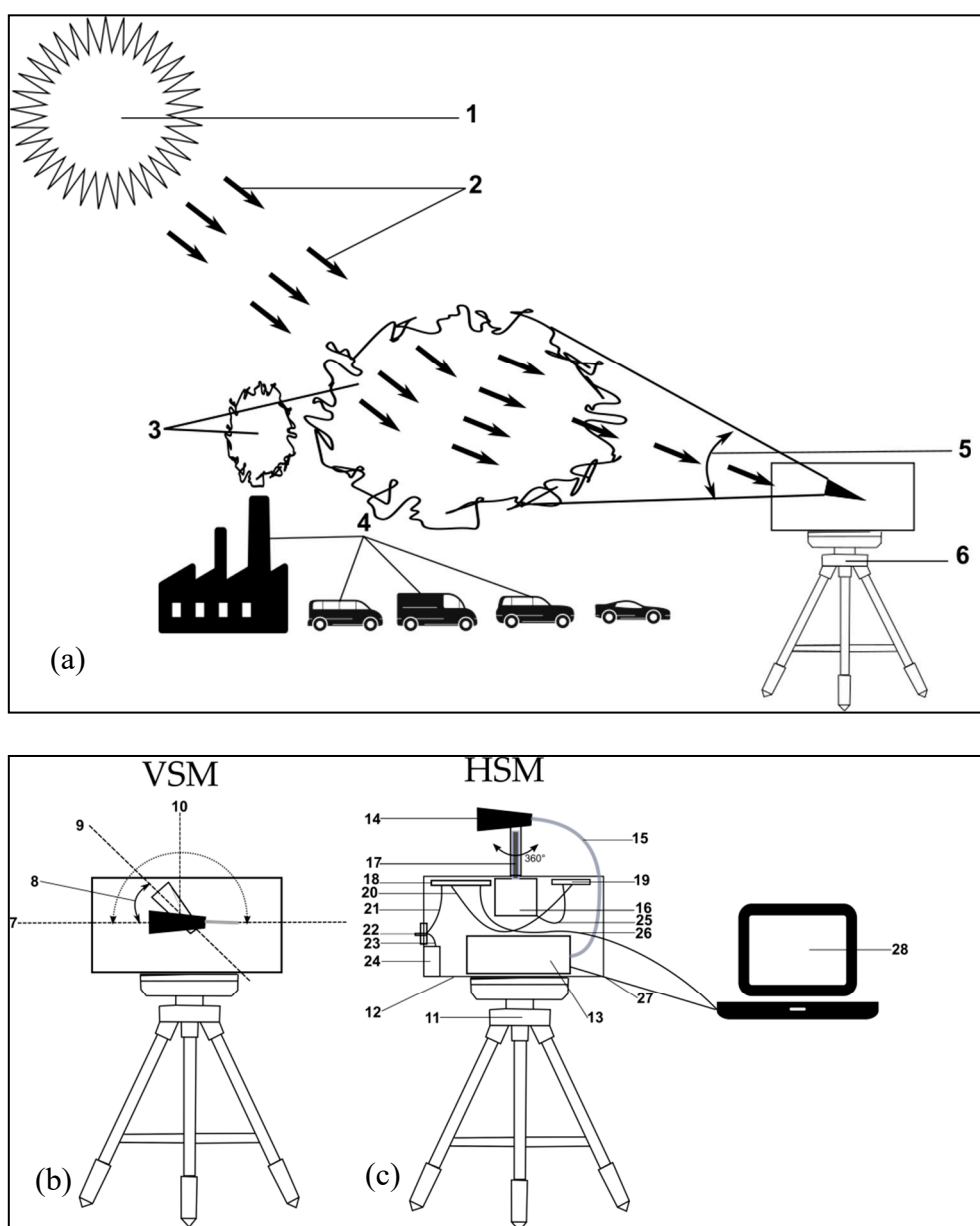


**Figure 2.** The UGAL-2-DOAS system. (a) Measurement principle: (1) radiation source; (2) radiation rays; (3) pollution plumes; (4) pollution sources; (5) field of view (FOV) of the device; (6) multi-axis differential optical absorption spectroscopy (MAX-DOAS) system. (b) Components and main characteristics of the scanning mode: (7). horizontal axis, (8) viewing angle (9) observation direction, (10), zenith; (c) Components: (11) tripod, (12) body, (13) ultraviolet–visible (UV–Vis) spectrometer; (14) telescope; (15) optic fiber; (17) mobile arm; (16) motor; (18) board; (19) electronic driver board; (20–23) electric connectors; (24) power switch; (25) accumulator; (26–27) communication cables; (28) storage unit.

Figure 2b shows the main characteristics of the scanning mode and components. The components of the new MAX-DOAS system are presented in Figure 2b. The body (12) houses the electronic elements of the device. The UV–Vis spectrometer (13) is the main component of the new MAX-DOAS system. A description of the main components of the UGAL-2D-DOAS system, as presented in Figure 2, are shown in Table 1. The UV–Vis spectrometer is an non-cooled Avantes AvaSpec-ULS2048 grating

spectrometer, according to the manufacturer this spectrometer is the best option when looking for a cost-effective and highly sensitive spectrometer. Table 2 presents the main technical characteristics of the Avantes UV-Vis spectrometer.

**Table 1.** The main components of the UGAL-2D-DOAS system.

Nr. *	Component	Description
13	UV-Vis spectrometer	Avantes AvaSpec-ULS2048, one channel Black baffle: internal diameter: 9 mm, length: 2 cm
14	Telescope (baffle+lens)	Avantes collimating lens; confocal length: 8.7 mm Telescope's field of view: 2.56° [4]
15	Optical fiber	Avantes 600 µm chrome plated brass optical fiber, 1 or 10 m length
16	Stepper motor	Nema 17 Stepper motor, 1.8°, 12 V
17	Mobile Arm	Metal piece
18	Micro Controller Board	Arduino UNO

\* Identification number as presented in Figure 2.

**Table 2.** The main technical characteristics of the Avantes UV-Vis spectrometer.

<b>Optical Bench</b>	symmetrical Czerny-Turner, 75 mm focal length
<b>Wavelength range</b>	200–550 nm
<b>Resolution</b>	0.7 nm
<b>Slit; Grating</b>	50 µm; 1200 L/mm
<b>Stray light</b>	<0.3%
<b>Sensitivity</b>	250,000 counts/µW per ms int. time
<b>Detector</b>	Back-thinned CCD <sup>1</sup> image sensor 2048 × 16 pixels, non-cooled
<b>Signal/Noise</b>	450:1
<b>Integration time</b>	1.82 ms–60 s
<b>Interface</b>	USB 2.0 high speed, 480 Mbps RS-232, 115,200 bps
<b>Data transfer speed</b>	1.82 ms/scan (USB2.0 <sup>2</sup> )
<b>Power supply</b>	Default USB power, or with SPU2 <sup>3</sup> external 12 V DC
<b>Dimensions; weight</b>	175 × 110 × 44 mm (1 channel), 855 g

<sup>1</sup> Charge-Coupled Device; <sup>2</sup> Universal Serial Bus; <sup>3</sup> Secondary Power Unit.

The Avantes AvaSpec-ULS2048 UV-Vis spectrometer is ideal for spectral detection of several atmospheric pollutants such as: NO<sub>2</sub>, SO<sub>2</sub>, or CH<sub>2</sub>O. This spectrometer was used during several experiments performed in Romania or international DOAS field campaigns such as AROMAT (Airborne Romanian Measurements of Aerosols and Trace gases) and AROMAPEX [23,24,30,35].

The system presented in this work is not waterproof but the spectrometer and control unit can be used indoors through a longer fiber optic and controlled through longer USB cables. Thus the system could be used for longer periods or in relatively bad weather conditions. The UGAL-2D-DOAS system is designed mainly for short-term DOAS field campaigns. Some similarities with other MAX-DOAS instruments, e.g., the CU 2-D-MAX-DOAS of Ortega et al. 2011 [34,36] do exist, but the main differences are related to the type of spectrometer used, telescope system and operation modes. The UGAL-2D-DOAS system can be set manually only to a single elevation angle during the azimuthal observations.

## 2.2. Observation Site

The new MAX-DOAS instrument was installed on the building rooftop of the Faculty of Science and Environment, Galati (Figure 3). This building is one of the highest in the observation area (35 m above ground) and no obstacles were encountered during the measurements. The city of Galati is located in South-East of Romania, has a population of ~250,000 inhabitants and a surface of ~250 km<sup>2</sup>. The major pollution sources are a steel factory and an oil factory (whose locations are shown in Figure 3) and road traffic [37–39]. Galati can be rated as a medium polluted city, where the maximum

tropospheric NO<sub>2</sub> vertical column density (VCD) content measured, e.g., by a mobile DOAS system, is  $\sim 1.5 \times 10^{16}$  molec./cm<sup>2</sup>. This value was recorded around the industrial area, located in the SW of Galati city [23,27].

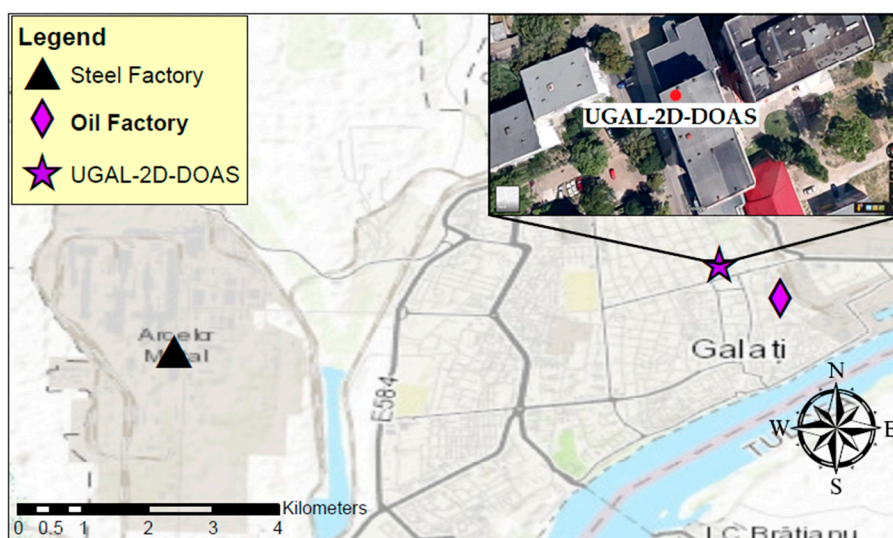


**Figure 3.** Location of the experiments using the UGAL-2D-DOAS system (image adapted from Google Earth [40] and ArcGIS v10.4).

### 2.3. Spectral Analysis

The DOAS technique uses UV–Vis scattered light as base for the retrieval of atmospheric trace gases content. The QDOAS software [41] was used to retrieve the information about the NO<sub>2</sub> content from all the spectra recorded by the new UGAL-2D-DOAS system. The QDOAS is a free and open source software which was used in many DOAS applications and studies [24,27]. Table 3 presents the QDOAS settings used during the spectral analysis. The wavelength calibration was performed using a highly resolved solar spectrum [42].

**Table 3.** The main settings used for the NO<sub>2</sub> spectral analysis.

Absorption Cross-Sections	Temperature	Fitting Window (nm)	Polynomial Order	Reference
NO <sub>2</sub>	298 K	425–495	5	[43]
O <sub>3</sub>	293 K	425–495	5	[44]
O <sub>4</sub>	293 K	425–495	5	[45]
Ring	N/A	425–495	5	[46]
H <sub>2</sub> O	296 K	425–495	5	[47]

The output of the spectral analysis is a differential slant column density (DSCD), which usually is expressed in molecules/cm<sup>2</sup>. The DSCD (Equation (1)) is basically the difference between the measured spectra (SCD<sub>meas</sub>) and the reference spectra (SCD<sub>ref</sub>) [27]. SCD<sub>ref</sub> is represented by a spectra recorded in zenith geometry under clear sky conditions at noon, for each day when measurements using the UGAL-2D-DOAS were performed. All the measurements presented in this work were performed under clear sky conditions. Figure 4 presents a typical NO<sub>2</sub> DOAS fit using a spectrum recorded during the experiments performed on 11 April 2017.

$$\text{DSCD} = \text{SCD}_{\text{meas}} - \text{SCD}_{\text{ref}} \quad (1)$$

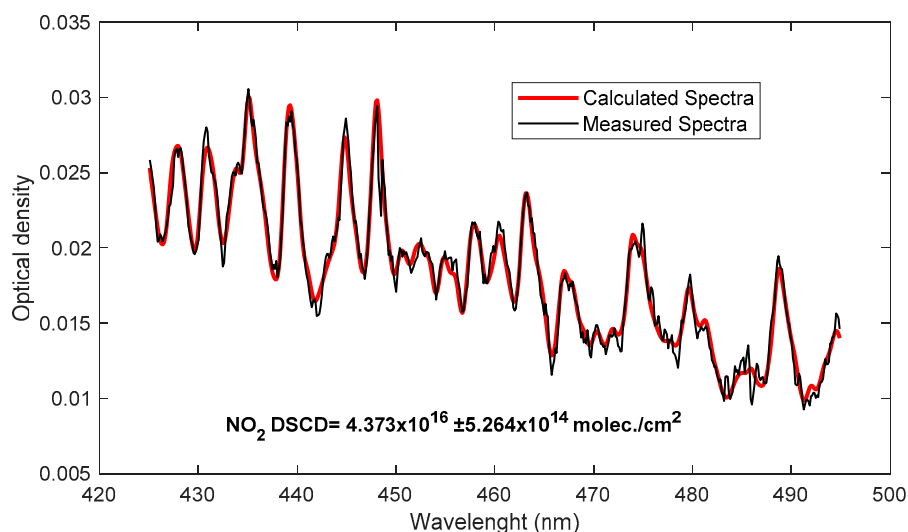


**Figure 4.** Example of a NO<sub>2</sub> DOAS fit realized with the QDOAS software; the analyzed spectrum was recorded on 4 November 2017, 10:02 local time (LT), horizontal scanning mode (HSM), Solar Zenith Angle = 55°; Red line represents the reference spectra and the black line represents the measured spectra.

### 3. Results and Discussions

#### 3.1. Horizontal Scanning Mode (HSM)

The first experiment using the UGAL-2D-DOAS system was conducted under the HSM (azimuthal observations) on 11 April 2017. The full azimuthal observations (0–360°) started from the North (0°), with a step of 9°, under 0° elevation during all tests. To validate and check the scanning sequence, after performing a full azimuthal scan, we performed several horizontal observations by blocking the starting point of the scan (0°) with a black block (BBox, 3 × 3 cm) placed at 5 cm in front of the MAX-DOAS telescope. After the first full azimuthal scanning, a second HSM was performed removing the BBox. Figure 5 shows the results of the with/without BBox experiment. Also, Figure 5 gives information about wind directions and velocity, which comes from the automatic weather station (Davis Vantage Pro2) located in the campus university of Galati city (45.44° N, 28.05° E). The weather station is located at 37 m height and acquires data every 10 min. During several horizontal scans we observed that each time, for the same position (0°), the new the MAX-DOAS instrument indicates mostly the dark current when the BBox was used. Because of the low wind conditions, and no important active NO<sub>2</sub> sources, the NO<sub>2</sub> DSCD is almost evenly distributed on the scan without the BBox (red line in Figure 5). The second scan, which includes the BBox, shows a variation of NO<sub>2</sub> DSCD located in the SE of the city, corresponding to a vegetable oil factory. The average values of the NO<sub>2</sub> DSCD recorded a range between 3–4 × 10<sup>16</sup> molec./cm<sup>2</sup>.

Figure 6 shows the NO<sub>2</sub> DSCD obtained from other two full HSM performed on 3 June 2017, at 14.00 and 15.00 local time (LT). During this experiment the wind was blowing from NE, and had an average speed of 8 m/s. A significant NO<sub>2</sub> content was detected by the UGAL-2D-DOAS system, 230–240° from North. The first NO<sub>2</sub> DSCD peak, recorded from 14 LT, account 4.97 × 10<sup>16</sup> molec./cm<sup>2</sup>, while the second NO<sub>2</sub> DSCD peak, recorded from 15 LT, account 3.97 × 10<sup>16</sup> molec./cm<sup>2</sup>. This high amount of NO<sub>2</sub> may be caused by the emissions of the steel factory, an important NO<sub>2</sub> source, located SW of the position of our MAX-DOAS instrument. The average NO<sub>2</sub> DSCD was around 1.5 × 10<sup>16</sup> molec./cm<sup>2</sup> during the entire scan except the sector where the plume is observed. A reduction from the average NO<sub>2</sub> content is observed towards NE, which can be associated with the less polluted area from NE, where only agricultural fields exist over a large area. This is supported by the very low NO<sub>2</sub> amount (>10<sup>16</sup> molec./cm<sup>2</sup>) in almost all directions except SW.

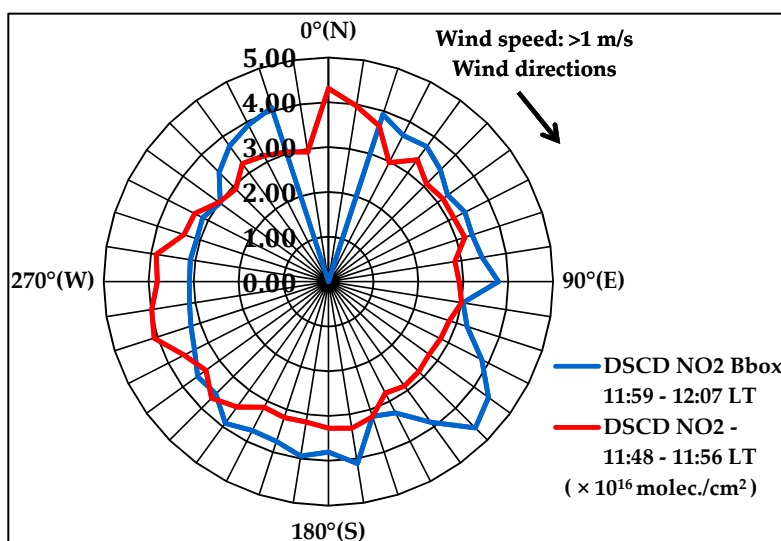


**Figure 5.** NO<sub>2</sub> DSCD results from 360° HSM and 0° elevation using the UGAL-2D-DOAS system in the black box (BBox) experiment on 11 April 2017. The blue line represents the NO<sub>2</sub> DSCD resulted from the full HSM using BBox as a field of view blocker to the North. The red line corresponds to the NO<sub>2</sub> DSCD resulted from the full HSM performed without the BBox.

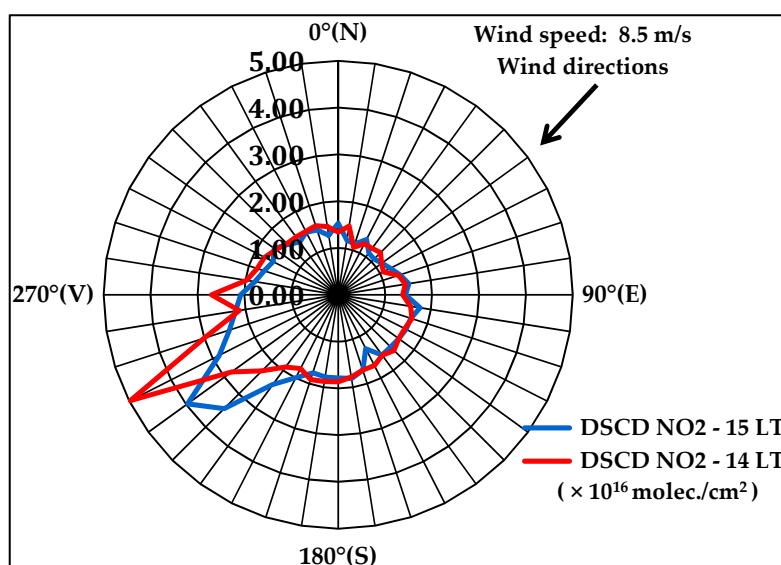


**Figure 6.** NO<sub>2</sub> differential slant column densities (DSCD) results using full 360° (HSM) by UGAL-2D-DOAS system on 3 June 2017.

### 3.2. Vertical Scanning Mode (VSM)

This section presents the results of elevation angle (VSM) sequence observations, which includes local celestial meridian observations.

Figure 7 shows results of the NO<sub>2</sub> DSCD measurements resulting from scans performed on 3 June 2017 in the VSM (local celestial meridian observations) that started at 12 LT, respective 13 LT. The MAX-DOAS instrument starts from North (i.e., 0°) and moves with a step-sequence of 9° to the South (180°), the 90° angle represents the zenith. The NO<sub>2</sub> content does not change during the two scans over the zenith sequence because the Sun is close to the time when reach its highest point in the sky. Also, Figure 7b shows the variation of O<sub>4</sub> DSCD detected during the celestial meridian observations performed on 3 June 2017.

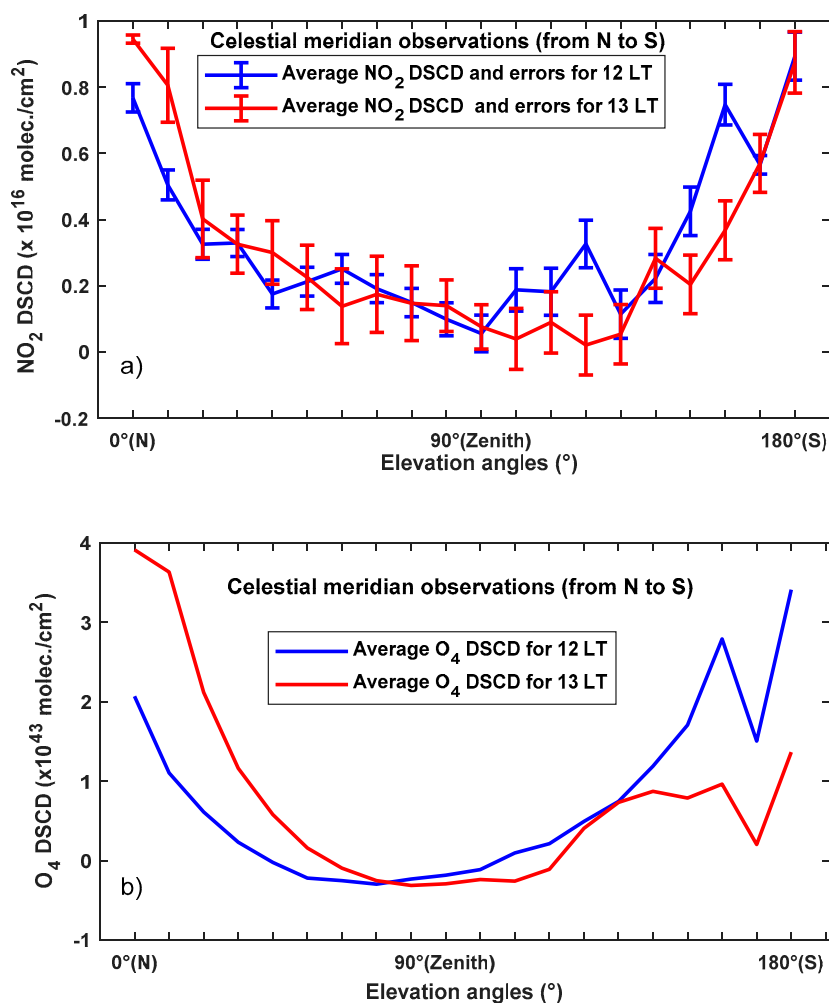


**Figure 7.** (a)  $\text{NO}_2$  DSCD and associated errors obtained from the UGAL-2D-DOAS system working in the vertical scanning mode (VSM), on 3 June 2017; and (b) the  $\text{O}_4$  DSCD for the same observations.

Figure 8 shows results of the UGAL-2D-DOAS measurements working in the VSM performed in the morning of 21 June 2017, between 6 and 10 LT. A complete local celestial scan (Figure 8, top) was followed by an East to West elevation angle sequence (Figure 8, bottom). A number of 6 or 7 complete sequences, each of 8 min, were performed during each hour. The scans were undertaken in the morning, when the Sun was relatively low, which explains the relatively high values of the  $\text{NO}_2$  DSCD compared to values for noon/afternoon seen in Figures 5–7. The observations performed from North–South (N–S) present a smaller variation, e.g., zenith  $\pm 40^\circ$ , compared to East–West (E–W) observations for the same elevation. The main reason is related to the fact that the industrial area of Galati city is located in the E and respective V sides of the city.

The  $\text{NO}_2$  DSCD is clearly highest at 6 LT, with an average value per VSM sequence of about  $2.92 \times 10^{16}$  molec./ $\text{cm}^2$  and constantly decreasing with time to a value of  $1.98 \times 10^{16}$  molec./ $\text{cm}^2$  at 9 LT, which is a consequence of the Solar Zenith Angle change. This was observed in both VSM observations (E–W and N–S), and confirms the capability of the instrument to detect relatively small variations of the  $\text{NO}_2$  DSCD in any direction. Also, Figure 8 show that the instrument is detecting almost the same values for the zenith observations, for both E–W and N–S scans, e.g., at 6 LT was observed  $1.68 \times 10^{16}$  molec./ $\text{cm}^2$  for E–W scan, versus  $1.64 \times 10^{16}$  molec./ $\text{cm}^2$  in N–S scan, and similar differences for the other three hours of observations. The small difference between the recorded values is caused by the rapid ascending of the Sun that occur at the time when the instrument was placed in order to perform scans in one direction (N–S) compared to the other (E–W).

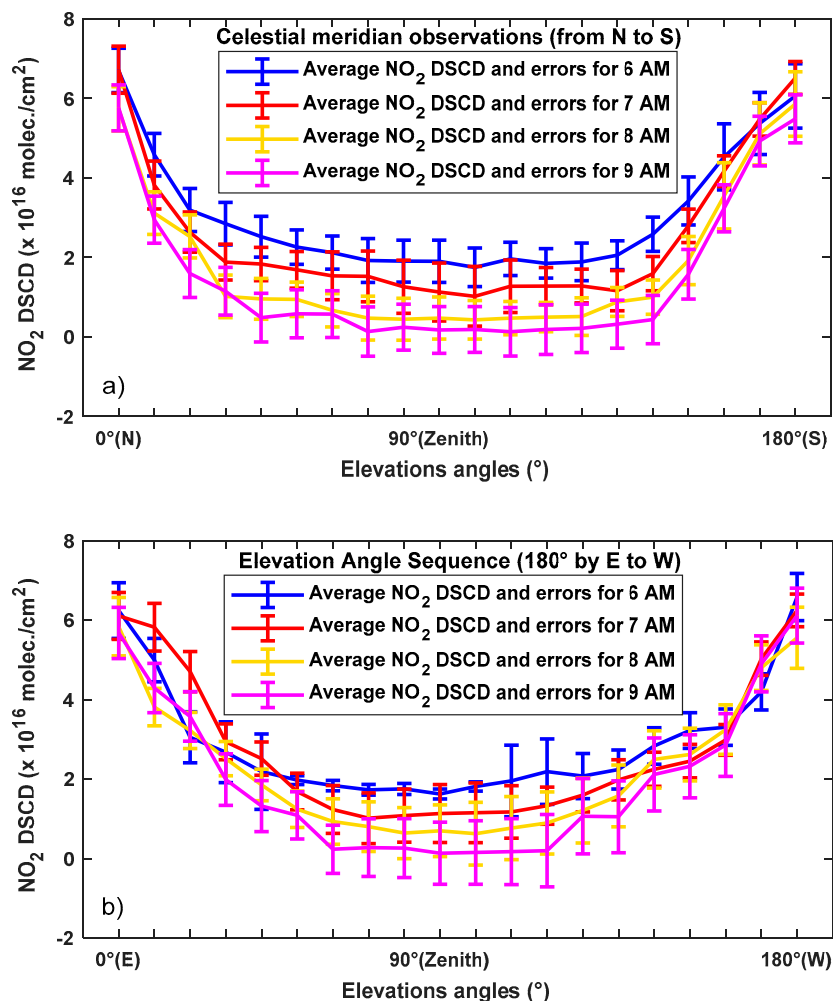


**Figure 8.** NO<sub>2</sub> DSCD and error retrieved from the VSM using the UGAL-2D-DOAS system on 21 June 2017 between 6–9 LT; (a) local celestial meridian; (b) elevation angle sequence (0–180° by E–W).

Table 4 summarizes the MAX-DOAS measurements for using HSM and VSM and associated errors.

**Table 4.** Information regarding the performed MAX-DOAS observations.

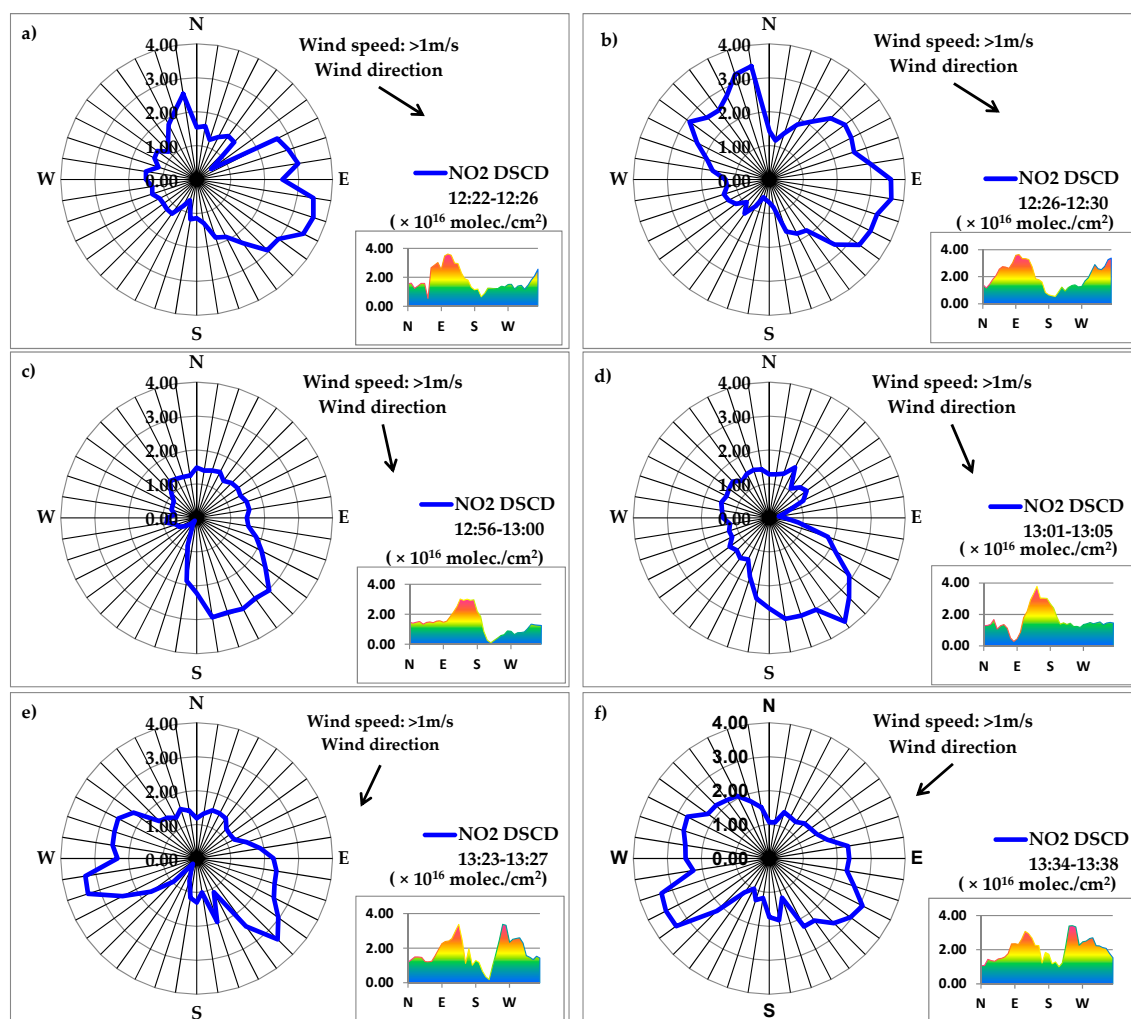
Scanning Mode	Date	Time Interval (LT)	Observations Per Sequence	Maximum NO <sub>2</sub> DSCD (×10 <sup>16</sup> molec./cm <sup>2</sup> )	The Error of NO <sub>2</sub> DSCD Min–Max (%)	Time Per Step (s)	Time Per Scan (min)
HSM	11 April 2017	10–11	40	4.62	1.15–6.93%	12	8
HSM	3 June 2017	14–15	40	4.97	1.03–5.81%	12	8
VSM	3 June 2017	12–13	20	0.95	1.59–4.54%	12	4
VSM	21 June 2017	06–09	20	1.94	1.5–6.5%	12	4
HSM	21 June 2017	12–14	40	3.88	1.0–9.64%	6	4

### 3.3. Comparison with Complementary Car Differential Optical Absorption Spectroscopy (Car-DOAS) Measurements

The NO<sub>2</sub> DSCD obtained from the measurements performed in HSM, using the UGAL-2D-DOAS system, were compared against the measurements obtained with a mobile-DOAS system. The results of the UGAL-2D-DOAS obtained using the HSM were improved by using a smaller integration time per determination, which allowed a full scan sequence in 4 min as can be seen in Table 2. The mobile system is a zenith-sky DOAS mounted on a car, whose results were validated through many studies and measurement campaigns [27,35]. Experiments involving the UGAL-2D-DOAS equipment and the mobile car-DOAS were made on 21 June 2017, between 12–14 LT. The first equipment worked in the

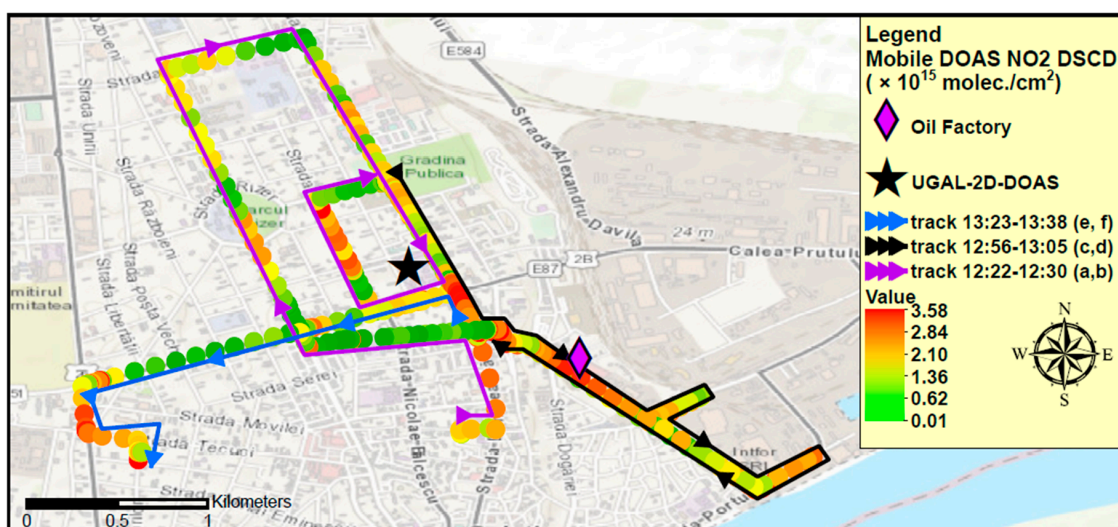
HSM, while the latter measured the DSCD along some of the main traffic lanes in Galati, in an area surrounding the stationary UGAL-2-DOAS system.

Figure 9a–f show the distribution of  $\text{NO}_2$  DSCDs retrieved, for some of the horizontal scans of the UGAL-2D-DOAS system done during 12–14 LT on 21 June 2017, as follows Figure 9a 12:22–12:26; Figure 9b 12:26–12:30; Figure 9c 12: 56–13:00; Figure 9d 13:01–13:05 Figure 9e 13:23–13:27; Figure 9f 13:34–13:38. In all plots, i.e., during the entire time of the experiment, a  $\text{NO}_2$  plume appears to the E-SE, with maxima of  $3.78 \times 10^{16}$  molec./ $\text{cm}^{-2}$ , at 13:02, and  $3.19 \times 10^{16}$  molec./ $\text{cm}^{-2}$ , at 12:57. Other peaks are observed to NNW during the first two intervals, i.e., between 12:22–12:30 (plots Figure 9a,b), reaching  $3.38 \times 10^{16}$  molec./ $\text{cm}^{-2}$ , and to the W-SW, of  $3.39 \times 10^{16}$  molec./ $\text{cm}^{-2}$ , in the last two plots (Figure 9e,f) between 13:23–13:38.



**Figure 9.** (a–f) The  $\text{NO}_2$  DSCD (blue line from radar type figures) obtained from the full azimuthal scans using UGAL-2D-DOAS system performed on 21 June 2017 for the following local time periods: (a)12:22–12:26; (b)12:26–12:30; (c)12: 56–13:00; (d)13:01–13:05 (e)13:23–13:27; (f) 13:34–13:38.

Figure 10 shows the position on the map of the stationary system (black star), considered as the reference point of the map, and the trajectory of the mobile DOAS system during intervals shown in Figure 9a–f, together with the corresponding  $\text{NO}_2$  DSCD. We aim here only at a qualitative comparison, and not at a point by point comparison, since large differences between absolute values of  $\text{NO}_2$  columns measured by the two systems are normal: the azimuthal measurements of UGAL-2-DOAS integrate the horizontal distribution of  $\text{NO}_2$  while the mobile, zenith-sky MAX-DOAS measurements integrate the vertical distribution of  $\text{NO}_2$ .



**Figure 10.** Map of spatial distribution of  $\text{NO}_2$  DSCD (circles) retrieved using the car-DOAS system on 21 June 2017, during 12–14 LT. The trajectory of mobile DOAS system is shown by arrows of different colors, corresponding to time intervals when the UGAL-2D-DOAS system was scanning. The location of the UGAL-2-DOAS system and of the oil factory are also shown; note that the position of the steel factory, which is  $\sim 6$  km away, cannot be included here for the sake of clarity of mobile DOAS resolution; (the map was created using ArcGIS v10.4).

During the first interval (12:22–12:30), the mobile DOAS detected high DSCDs (of about  $3.5\text{--}4 \times 10^{15}$  molec./ $\text{cm}^{-2}$ ) around the SE and to the W-NW of the stationary system. Also, smaller increases of the DSCD are seen along the streets N-NNW of the stationary system (of about  $2.5 \times 10^{15}$  molec./ $\text{cm}^{-2}$ ). The maxima observed by the car-DOAS are similar to what UGAL-2D-DOAS observed. However, the plume observed by the stationary system is not seen in the car-DOAS results because the car did not reach any street to the East of the stationary system. However, measurements done at later times and a visual inspection of the horizon (see photo in the Appendix A) suggest that the plume is caused by emissions of a point source which is the oil factory, showed in the map by the purple diamond in Figure 10. The traffic for first track, especially for the streets in the NW part of the map, is not crowded, thus there is no clear explanation for the peak in  $\text{NO}_2$  along these streets. One cause may be that some wind gust, blowing from the SE carried some of the oil-factory emissions to the western part of the city. Unfortunately we do not have minute-resolution wind measurements to confirm this assumption.

During the second interval of the mobile observations (12:56–13:05) the plume detected by UGAL-2D-DOAS over the SE is clearly supported by zenith-sky car-DOAS observations which give DSCDs around  $4 \times 10^{15}$  molec./ $\text{cm}^{-2}$ , which is the highest  $\text{NO}_2$  amount detected by mobile DOAS on 21 June 2017. The traffic here is not particularly high, thus the increased  $\text{NO}_2$  content can be mostly attributed to the oil factory. Interestingly, during the last interval (13:23–13:38) the mobile DOAS observations support both DSCD peaks observed by the UGAL-2-DOAS as shown in Figure 8e,f: the  $\text{NO}_2$  content is higher to SE (which may be the result of emissions of the oil factory) and WSW of the stationary DOAS system. The latter pollution increase may be due to emissions from the steel factory (whose position is not included here for the sake of clarity of mobile DOAS resolution, but is shown in Figure 3).

#### 4. Conclusions

We described here a low-cost MAX-DOAS system, developed at the “Dunarea de Jos” University of Galati, Romania, named UGAL-2D-DOAS. The new MAX-DOAS system was developed to measure atmospheric  $\text{NO}_2$  and other several trace gas content, being designed mainly for short-term DOAS field campaigns. The new MAX-DOAS instrument is able to perform measurements using full azimuthal

(HSM, 0–360°), celestial meridian observations, and other elevation angle sequences (VSM, 0–180°). The capabilities of the equipment were tested (1) using both scanning modes and (2) comparing the MAX-DOAS observations with measurements of a reliable zenith-sky DOAS system. We found that the new MAX-DOAS system is able to detect diurnal variation or local NO<sub>2</sub> urban or industrial emissions, when being used under 360° azimuthal mode (HSM) and celestial meridian observation or other elevation angle sequence (e.g., VSM by E-W). The NO<sub>2</sub> DSCD retrieved from the UGAL-2D-DOAS system was compared to coincident NO<sub>2</sub> DSCD measurements performed by a zenith-sky car-DOAS equipment, in the area surrounding the location of the static MAX-DOAS instrument. Comparisons between results of the two DOAS systems have shown that the new MAX-DOAS instrument can identify NO<sub>2</sub> hot-spots and variability at a range of at least 1 km.

We found that our system can detect and quantify NO<sub>2</sub> atmospheric content, but the determination of concentrations requires a more complex approach that will be included in future studies. The calculation of the vertical column density (VCD) and the associated air mass factor (AMF) will be part of future work. Also, the new MAX-DOAS instrument will be tested in future national and international DOAS campaigns. The major advantage of the in-house equipment is that the new optic system is a low-cost solution against the existing market of the MAX-DOAS systems, considering that main costs are represented by the UV–Vis spectrometer.

**Author Contributions:** Conceptualization, A.R., D.-E.C. and M.A.; Formal analysis, D.-E.C.; Investigation, A.R., D.-E.C. and M.V.; Methodology, A.R.; Validation, D.-E.C.; Writing—original draft, A.R. and M.V.; Writing—review & editing, D.-E.C., M.V., A.M., M.V.R. and P.L.G. All authors have read and agreed to the published version of the manuscript.

**Funding:** The work of A.R. and M.A. was supported by the project ANTREPRENORDOC, in the framework of Human Resources Development Operational Programme 2014–2020, financed from the European Social Fund under the contract number 36355/23.05.2019 HRD OP /380/6/13—SMIS Code: 123847. The work of M.V. and P.L.G. was supported by the project “EXPERT”, financed by the Romanian Ministry of Research and Innovation, Contract no. 14PFE/17.10.2018.

**Conflicts of Interest:** The authors declare no conflict of interest.

## Appendix A



**Figure A1.** Photography of the oil factory emissions observed by both DOAS systems, city (13:06 21 June 2017).

## References

1. Dobson, G.M.; Harrison, D.N. Measurements of the Amount of Ozone in the Earth's Atmosphere and its Relation to Other Geophysical Conditions. In *Proceedings of the Royal Society of London. Series A, Containing Papers of a Mathematical and Physical Character*; Royal Society: London, UK, 1926; Volume 110, pp. 660–693.
2. Dobson, G.M.B.; Kimball, H.H.; Kidson, E. Observations of the Amount of Ozone in the Earth's Atmosphere, and Its Relation to Other Geophysical Conditions. Part IV. *Proc. R. Soc. A Math. Phys. Eng. Sci.* **1930**, *129*, 411–433. [[CrossRef](#)]
3. Noxon, J.F. Nitrogen dioxide in the stratosphere and troposphere measured by ground-based absorption spectroscopy. *Science* **1975**, *189*, 547–549. [[CrossRef](#)] [[PubMed](#)]
4. Merlaud, A. *Development and Use of Compact Instruments for Tropospheric Investigations Based on Optical Spectroscopy from Mobile Platforms*; Presses univ. de Louvain: Louvain-la-Neuve, Belgium, 2013; p. 307.
5. Hönninger, G.; von Friedeburg, C.; Platt, U. Multi Axis Differential Optical Absorption Spectroscopy (MAXDOAS). *Atmos. Chem. Phys.* **2004**, *4*, 231–254. [[CrossRef](#)]
6. Arpag, K.H.; Johnston, P.V.; Miller, H.L.; Sanders, R.W.; Solomon, S. Observations of the stratospheric BrO column over Colorado, 40° N. *J. Geophys. Res.* **1994**, *99*, 8175–8181. [[CrossRef](#)]
7. Seitz, K.; Buxmann, J.; Pöhler, D.; Sommer, T.; Tschirner, J.; Neary, T.; O'Dowd, C.; Platt, U. The spatial distribution of the reactive iodine species IO from simultaneous active and passive DOAS observations. *Atmos. Chem. Phys.* **2010**, *10*, 2117–2128. [[CrossRef](#)]
8. Solomon, S.; Schmeltekopf, A.L.; Sanders, R.W. On the interpretation of zenith sky absorption measurements. *J. Geophys. Res.* **1987**, *92*, 8311–8319. [[CrossRef](#)]
9. Wittrock, F.; Müller, R.; Richter, A.; Bovensmann, H.; Burrows, J.P. Measurements of Iodine monoxide (IO) above Spitsbergen. *Geophys. Res. Lett.* **2000**, *27*, 1471–1474. [[CrossRef](#)]
10. Richter, A.; Eisinger, M.; Ladstätter-Weissenmayer, A.; Burrows, J.P. DOAS zenith sky observations: 2. Seasonal variation of BrO over Bremen (53° N) 1994–1995. *J. Atmos. Chem.* **1999**, *32*, 83–99. [[CrossRef](#)]
11. Heckel, A.; Richter, A.; Tarsu, T.; Wittrock, F.; Hak, C.; Pundt, I.; Junkermann, W.; Burrows, J.P. MAX-DOAS measurements of formaldehyde in the Po-Valley. *Atmos. Chem. Phys. Discuss.* **2005**, *5*, 909–918. [[CrossRef](#)]
12. Platt, U.; Stutz, J. Differential Absorption Spectroscopy. In *Physics of Earth and Space Environments*; Springer: Berlin, Germany, 2008. [[CrossRef](#)]
13. Javez, Z.; Lui, C.; Ullah, K.; Xing, C.H.; Lui, H. Investigating the effect of different meteorological conditions on MAX-DOAS observations of NO<sub>2</sub> and CHOCHO in Hefei, China. *Atmosphere* **2019**, *10*, 353. [[CrossRef](#)]
14. Platt, U.; Hönninger, G. The role of halogen species in the troposphere. *Chemosphere* **2003**, *52*, 325–338. [[CrossRef](#)]
15. Leser, H.; Hönninger, G.; Platt, U. MAX-DOAS measurements of BrO and NO<sub>2</sub> in the marine boundary layer. *Geophys. Res. Lett.* **2003**, *30*, 1537. [[CrossRef](#)]
16. Wang, Y.; Beirle, S.; Hendrick, F.; Hilboll, A.; Jin, J.; Kyuberis, A.A.; Lampel, J.; Li, A.; Luo, Y.; Lodi, L.; et al. MAX-DOAS measurements of HONO slant column densities during the MAD-CAT campaign: Inter-comparison, sensitivity studies on spectral analysis settings, and error budget. *Atmos. Meas. Tech.* **2017**, *10*, 3719–3742. [[CrossRef](#)]
17. Bobrowski, N.; Platt, U. SO<sub>2</sub>/BrO ratios studied in five volcanic plumes. *J. Volcanol. Geotherm. Res.* **2007**, *166*, 147–160. [[CrossRef](#)]
18. Trebs, I.; Meixner, F.X.; Slanina, J.; Otjes, R.; Jongejan, P.; Andreae, M.O. Erratum: Real-time measurements of ammonia, acidic trace gases and water-soluble inorganic aerosol species at a rural site in the Amazon Basin. *Atmos. Chem. Phys.* **2005**, *4*, 967–987. [[CrossRef](#)]
19. Hönninger, G.; Leser, H.; Sebastián, O.; Platt, U. Ground-based measurements of halogen oxides at the Hudson Bay by active longpath DOAS and passive MAX-DOAS. *Geophys. Res. Lett.* **2004**, *31*, L04111. [[CrossRef](#)]
20. Wagner, T.; Dix, B.V.; Friedeburg, C.V.; Frieß, U.; Sanghavi, S.; Sinreich, R.; Platt, U. MAX-DOAS O<sub>4</sub> measurements: A new technique to derive information on atmospheric aerosols—Principles and information content. *J. Geophys. Res. D Atmos.* **2004**, *109*, 1–19. [[CrossRef](#)]
21. Johansson, M.E.; Rivera, C.; de Foy, B.; Lei, W.; Song, J.; Zhang, Y.; Galle, B.; Molina, L.T. Mobile mini-DOAS measurement of the outflow of NO<sub>2</sub> and HCHO from Mexico City. *Atmos. Chem. Phys.* **2009**, *9*, 5647–5653. [[CrossRef](#)]

22. Schreier, S.; Peters, E.; Richter, A.; Lampel, J.; Wittrock, F.; Burrows, J. Ship-based MAX-DOAS measurements of tropospheric NO<sub>2</sub> and SO<sub>2</sub> in the South China and Sulu Sea. *Atmos. Environ.* **2015**, *102*, 331–343. [[CrossRef](#)]
23. Constantin, D.E.; Merlaud, A.; Voiculescu, M.; Dragomir, C.; Georgescu, L.; Hendrick, F.; Pinardi, G.; Van Roozendaal, M. Mobile DOAS observations of tropospheric NO<sub>2</sub> using an ultralight trike and flux calculation. *Atmosphere (Basel)* **2017**, *4*, 78. [[CrossRef](#)]
24. Tack, F.; Merlaud, A.; Meier, A.C.; Vlemmix, T.; Ruhtz, T.; Iordache, M.-D.; Ge, X.; van der Wal, L.; Schuettemeyer, D.; Ardelean, M.; et al. Intercomparison of four airborne imaging DOAS systems for tropospheric NO<sub>2</sub> mapping—The AROMAPEX campaign. *Atmos. Meas. Tech.* **2019**, *12*, 211–236. [[CrossRef](#)]
25. Rivera, C.; Barrera, H.; Grutter, M.; Zavala, M.; Galle, B.; Bei, N.; Li, G.; Molina, L.T. NO<sub>2</sub> fluxes from Tijuana using a mobile mini-DOAS during Cal-Mex 2010. *Atmos. Environ.* **2013**, *70*, 532–539. [[CrossRef](#)]
26. Ionov, D.; Poberovskii, A. Quantification of NO<sub>x</sub> emission from St Petersburg (Russia) using mobile DOAS measurements around the entire city. *Int. J. Remote. Sens.* **2015**, *36*, 2486–2502. [[CrossRef](#)]
27. Constantin, D.E.; Merlaud, A.; Van Roozendaal, M.; Voiculescu, M.; Fayt, C.; Hendrick, F.; Pinardi, G.; Georgescu, L. Measurements of tropospheric NO<sub>2</sub> in Romania using a zenith-sky mobile DOAS system and comparisons with satellite observations. *Sensors* **2013**, *13*, 3922–3940. [[CrossRef](#)] [[PubMed](#)]
28. Constantin, D.E.; Merlaud, A.; Voiculescu, M.; Van Roozendaal, M.; Arseni, M.; Rosu, A.; Georgescu, L. NO<sub>2</sub> and SO<sub>2</sub> observations in southeast Europe using mobile DOAS observations. *Carpathian J. Earth Environ. Sci.* **2017**, *12*, 323–328.
29. Shaiganfar, R.; Beirle, S.; Petetin, H.; Zhang, Q.; Beekmann, M.; Wagner, T. New concepts for the comparison of tropospheric NO<sub>2</sub> column densities derived from car-MAX-DOAS observations, OMI satellite observations and the regional model CHIMERE during two MEGAPOLI campaigns in Paris 2009/10. *Atmos. Meas. Tech.* **2015**, *8*, 2827–2852. [[CrossRef](#)]
30. Carlos, M.A.; Schönhardt, A.; Bösch, T.; Richter, A.; Seyler, A.; Philip, B.J.; Ruhtz, T.; Constantin, D.; Georgescu, L.; Shaiganfar, R.; et al. High-resolution airborne imaging DOAS measurements of NO<sub>2</sub> above Bucharest during AROMAT. *Atmos. Meas. Tech.* **2017**, *10*, 1831–1857. [[CrossRef](#)]
31. Merlaud, A.; Tack, F.; Constantin, D.; Georgescu, L.; Maes, J.; Fayt, C.; Mingireanu, F.; Schuettemeyer, D.; Meier, A.C.; Ruhtz, T. The small whiskbroom imager for atmospheric composition monitoring (SWING) and its operations from an unmanned aerial vehicle (UAV) during the AROMAT campaign. *Atmos. Meas. Tech.* **2018**, *11*, 551–567. [[CrossRef](#)]
32. Dragomir, C.M.; Constantin, D.E.; Voiculescu, M.; Georgescu, L.P.; Merlaud, A.; Van Roozendaal, M. Modeling results of atmospheric dispersion of NO<sub>2</sub> in an urban area using METI-LIS and comparison with coincident mobile DOAS measurements. *Atmos. Pollut. Res.* **2015**, *6*, 503–510. [[CrossRef](#)]
33. Schreier, S.F.; Richter, A.; Burrows, J.P. Near-surface and path-averaged mixing ratios of NO<sub>2</sub> derived from car DOAS zenith-sky and tower DOAS off-axis measurements in Vienna: A case study. *Atmos. Chem. Phys.* **2019**, *19*, 5853–5879. [[CrossRef](#)]
34. Ortega, I.; Koenig, T.; Sinreich, R.; Thomson, D.; Volkamer, R. The CU 2-D-MAX-DOAS instrument—Part 1: Retrieval of 3-D distributions of NO<sub>2</sub> and azimuth-dependent OVOC ratios. *Atmos. Meas. Tech.* **2015**, *8*, 2371–2395. [[CrossRef](#)]
35. Constantin, D.E.; Merlaud, A.; the AROMAT team. AROMAT-I Final Report ESA Study: “Airborne Romanian Measurements of Aerosols and Trace Gases”. 2016. ESA Contract No.4000113511/NL/FF/gp. Available online: <https://earth.esa.int/documents/10174/134665/AROMAT-2-Final-Report> (accessed on 22 January 2020).
36. Coburn, S.; Dix, B.; Sinreich, R.; Volkamer, R. The CU ground MAX-DOAS instrument: Characterization of RMS noise limitations and first measurements near Pensacola, FL of BrO, IO, and CHOCHO. *Atmos. Meas. Tech.* **2011**, *4*, 2421–2439. [[CrossRef](#)]
37. Constantin, D.E.; Voiculescu, M.; Georgescu, L.; Trif, C.; Karakolios, E.; Mamoukaris, A.; Xipolitos, K. Imprint of road vehicles dynamics on atmospheric pollution. case study: Bucharest city 2007–2010. *J. Environ. Prot. Ecol.* **2012**, *13*, 837–843.
38. Constantin, D.E.; Voiculescu, M.; Georgescu, L. Satellite Observations of NO<sub>2</sub> Trend over Romania. *Sci. World J.* **2013**, 261634. [[CrossRef](#)]
39. Rosu, A.; Rosu, B.; Arseni, M.; Constantin, D.E.; Voiculescu, M.; Georgescu, L.P.; Van Roozendaal, M. Tropospheric nitrogen dioxide measurements in South-East of Romania using zenith-sky mobile DOAS observations. *Teh-New Technol. Prod. Mach. Manuf. Technol.* **2017**, *44*, 189–194.

40. Google Maps. Available online: <https://www.google.ro/maps/@45.4472707,28.0515216,184a,35y,174.06h/data=!3m1!1e3> (accessed on 7 July 2017).
41. Danckaert, T.; Fayt, C.; Van Roozendaal, M.; De Smedt, I.; Letocart, V.; Merlaud, A.; Pinardi, G. *QDOAS Software User Manual*; Version 3; Royal Belgian Institute for Space Aeronomy: Bruxelles, Belgium, 2013.
42. Kurucz, H.L. The Solar Spectrum: Atlases and Line Identifications. In *Laboratory and Astronomical High Resolution Spectra*; Sauval, A.J., Blomme, R., Grevesse, N., Eds.; Astronomical Society of the Pacific: San Francisco, CA, USA, 1995; Volume 81, pp. 17–31.
43. Vandaele, A.C.; Hermans, C.; Simon, P.C.; Carleer, M.; Colin, R.; Fally, S.; Merienne, M.F.; Jenouvrier, A.; Coquart, B. Measurements of the NO<sub>2</sub> absorption cross-section from 42,000 cm<sup>-1</sup> to 10,000 cm<sup>-1</sup> (238–1000 nm) at 220 K and 294 K. *J. Quant. Spectrosc. Radiat. Transf.* **1998**, *59*, 171–184. [[CrossRef](#)]
44. Bogumil, K.; Orphal, J.; Burrows, J.P. *Temperature dependent absorption cross sections of O<sub>3</sub>, NO<sub>2</sub>, and other atmospheric trace gases measured with the SCIAMACHY spectrometer. Proceedings of the ERS-Envisat-Symposium, Goteborg, Sweden. 16–20 October*; European Space Agency: Paris, France, 2000.
45. Thalman, R.; Volkamer, R. Temperature dependent absorption cross-sections of O<sub>2</sub>-O<sub>2</sub> collision pairs from 340–630 nm. *Phys. Chem. Chem. Phys.* **2013**, *15*, 15371–15381. [[CrossRef](#)]
46. Chance, K.V.; Spurr, R.J.D. Ring effect studies: Rayleigh scattering, including molecular parameters for rotational Raman scattering, and the Fraunhofer spectrum. *Appl. Opt.* **1997**, *36*, 5224–5230. [[CrossRef](#)]
47. Rothman, L.S.; Gordon, I.E.; Barber, R.J.; Dothe, H.; Gamache, R.R.; Goldman, A.; Perevalov, V.I.; Tashkun, S.A.; Tennyson, J. HITEMP, the high-temperature molecular spectroscopic database. *J. Quant. Spectrosc. Radiat. Transf.* **2010**, *111*, 2139–2150. [[CrossRef](#)]



© 2020 by the authors. Licensee MDPI, Basel, Switzerland. This article is an open access article distributed under the terms and conditions of the Creative Commons Attribution (CC BY) license (<http://creativecommons.org/licenses/by/4.0/>).